Airy-like pulses in models of large molecular chains, and conservative numerical methods for quasi-linear Hamiltonian systems

Brenton LeMesurier

*Department of Mathematics, College of Charleston, South Carolina**

(Dated: January 15, 2013)

Abstract

The phenomenon of coherent energetic pulse propagation in macromolecular chains such as α-helix protein is studied using the Davydov-Scott model, with both numerical studies using a new unconditionally stable fourth order accurate energy-momentum conserving time discretization, and with analysis based on ideas of center manifold theory.

It is shown that for physically natural impulsive initial data, the coherent traveling pulses seen have a form related to the Airy function, but with rapid variation of phase along the chain. This can be explained in terms of a new continuum limit approximation by the third derivative nonlinear Schrödinger equation, which differs from the previous continuum limit approximations related to the standard NLS equation.

A theorem is given describing the construction of such conservative time discretizations for a large class of Hamiltonian systems.

PACS numbers: 87.10.Ed, 87.10.Hk, 87.14.Ex, 87.14.et, 87.15.Ax, 87.15.ap

Keywords: Davydov-Scott system, conservative time-discretization

* Currently visiting CSCAMM, University of Maryland, and the Department of Mathematical Sciences, George Mason University.; lemesurierb@cofc.edu; http://blogs.cofc.edu/lemesurierb/

I. INTRODUCTION

A. Exciton-Oscillator Models of Macromolecular Chains

Various phenomena in macromolecular chains, such as proteins and DNA, are modeled by large systems of ODE's in Hamiltonian form, with conservation of energy and possibly some quadratic invariants, here called "momenta". In particular, many such models, along with spatial discretizations of various nonlinear wave equations, involve *exciton-oscillator* systems

$$\begin{aligned} \mathrm{i}\frac{d\psi_n}{dt} + \sum_s L_s \psi_{n+s} &= \sum_\nu \chi_{\nu,n} q_\nu \psi_n, \\ m\frac{d^2 q_\nu}{dt^2} + \sum_s \Omega_s q_{\nu+s} &= -\sum_n |\psi_n|^2, \end{aligned} \tag{1}$$

with symmetry conditions $L_{-s} = L_s$, $\Omega_{-s} = \Omega_s$. These have Hamiltonian form

$$\mathcal{H} = \sum_{n,s} L_s(\psi_n^* \psi_{n+s} + \psi_{n+s}^* \psi_n) + \sum_\nu \frac{p_\nu^2}{2m} + \frac{1}{2}\sum_{\nu,s} \Omega_s q_\nu + \sum_{\nu,n} q_\nu \psi_n^* \psi_n, \tag{2}$$

$$\mathrm{i}\frac{d\psi_n}{dt} = \frac{\partial \mathcal{H}}{\partial \psi_n^*}, \quad \mathrm{i}\frac{d\psi_n^*}{dt} = -\frac{\partial \mathcal{H}}{\partial \psi_n}, \tag{3}$$

$$\frac{dq_\nu}{dt} = \frac{\partial \mathcal{H}}{\partial p_\nu}, \quad \frac{dp_\nu}{dt} = -\frac{\partial \mathcal{H}}{\partial q_\nu}. \tag{4}$$

Note that ψ_n and ψ_n^* are here treated formally as independent variables, but in practice they are complex conjugates, the Hamiltonian is real, and so only the first equation in (3) is needed.

There is also a related class of Lattice Nonlinear Schrödinger [LNLS] equation models

$$\mathrm{i}\frac{d\psi_n}{dt} + \sum_s L_s \psi_{n+s} = 2\sum_s \chi_s |\psi_{n+s}|^2 \psi_n \tag{5}$$

with Hamiltonian

$$\mathcal{H} = \sum_{n,s} L_s \psi_n^* \psi_{n+s} + \sum_{n,s} \chi_s |\psi_n|^2 |\psi_{n+s}|^2. \tag{6}$$

Section II introduces the main example considered here, one developed by Alexandr Davydov, Alwyn Scott et al [1–5] for energy propagation in α-helix protein, which is the dominant helical form occurring in parts of protein molecules

$$\begin{aligned} \mathrm{i}\frac{d\psi_n}{dt} + J(\psi_{n-3} + \psi_{n+3}) - L(\psi_{n-1} + \psi_{n+1}) &= (q_{n+3} - q_n)\psi_n, \\ m\frac{d^2 q_n}{dt^2} - (q_{n-3} - 2q_n + q_{n+3}) &= |\psi_n|^2 - |\psi_{n-3}|^2, \end{aligned} \tag{7}$$

along with a lattice NLS approximation thereof,

$$\mathrm{i}\frac{d\psi_n}{dt} + J(\psi_{n+3} + \psi_{n-3}) - L(\psi_{n+1} + \psi_{n-1}) + |\psi_n|^2\psi_n = 0. \tag{8}$$

The physical meaning and parameter values are discussed further in the next section.

Many of the methods and results here also apply to related models as described in surveys by Davydov [6] and Scott [7], and considered for example in the more recent work of Ivić et al [8–10].

B. Numerical Observations and Analysis

Section III introduces a new fourth order accurate time-discretization method that exactly conserves the Hamiltonian ("energy") and all quadratic invariants ("momenta"), with unconditional stability to handle the stiffness that can arise. A difference calculus procedure is described for constructing such time discretizations with conservation of all quadratic invariants as well as the energy (Hamiltonian).

This discrete gradient method adapts easily to model refinements such as stochastic modeling of interactions with the aqueous environment and more accurate modeling of intramolecular forces, and to related questions such as signal propagation in DNA. The order of accuracy can easily be increased when this is desirable.

Section IV then applies this method in numerical studies that partially confirm previous observations and conjectures that sustained pulses can carry energy further and with less dispersion than one might expect from linearized approximations. However, a previous continuum limit approximation in terms of the nonlinear Schrödinger [NLS] equation and its sech soliton traveling wave solutions is shown to be invalid for typical initial data, due to a fast variation of the phase along the chain.

Instead, it is shown in Section V that the coherent pulse phenomenon seen is in part approximated by a new continuum limit, in terms of the third derivative nonlinear Schrödinger equation, having the Airy PDE as its linear part. The pulse structure is related to solutions of it'd linearization, the Airy PDE, which are in terms of the Airy function. With larger initial data, and thus stronger nonlinear effects, the pulse becomes more unimodal, with great concentration of signal strength in leading pulse with amplitude of roughly sech form, thus becoming reminiscent of NLS solitons.

II. THE DAVYDOV-SCOTT MODEL OF α-HELIX PROTEIN AND LATTICE NLS APPROXIMATION

Davydov et al proposed a model of excitation propagation in α-helix protein in [1, 2]. The version (7) of the model used here is based on refinements introduced by Scott in [3–5] which reflect newer experimental measurements. This model also neglects a variety of weaker interact terms described in [3], and most physical parameters have been scaled away, leaving three time scales

$$J \approx 1.4 \text{ THz}, \quad L \approx 2.3 \text{ THz}, \quad \omega = \sqrt{1/m} \approx 12 \text{ THz}.$$

See also the surveys and references in [6, 7, 11, 12], and the similar earlier modeling by Holstein [13, 14].

The index n labels the amino acid residues. However, the helical structure is reflected by a repeating unit cell consisting of three consecutive residues, with total rotation of close to one full turn of the helix. Thus the physical structure is made clearer by indexing each unit cell by ν, and the three residues within a unit cell with $\alpha = 0, 1, 2$ (so that $n = 3\nu + \alpha$), so occasionally the variables are labeled $\psi_{\nu,\alpha} = \psi_n$ and so on:

$$\begin{aligned} \mathrm{i}\frac{d\psi_{\nu,\alpha}}{dt} + J(\psi_{\nu-1,\alpha} + \psi_{\nu+1,\alpha}) - L(\psi_{\nu,\alpha-1} + \psi_{\nu,\alpha+1}) &= (q_{\nu+1,\alpha} - q_{\nu,\alpha})\psi_{\nu,\alpha}, \\ m\frac{d^2 q_{\nu,\alpha}}{dt^2} - (q_{\nu-1,\alpha} - 2q_{\nu,\alpha} + q_{\nu+1,\alpha}) &= |\psi_{\nu,\alpha}|^2 - |\psi_{\nu-1,\alpha}|^2. \end{aligned} \tag{9}$$

The three substructures of residues with equal index α are almost linear and these are called *spines*: note that most interactions are along these spines.

The Variables

- The *exciton* variables ψ_n (coming from reduction of Schrödinger's equation) give the probability that the C=O double bond in amino acid residue n is in a vibrational excited state.

- The position variables q_n are the displacements of the residues from rest position, in the direction of the axis of the helix: that is, along spines. The corresponding momenta are $p_n = m\, dq_n/dt$.

- Parameter J measures the (attractive) interaction between excitons in residues that are adjacent along a *spine*.
- Parameter L measures the (repulsive) interaction between excitons in residues that are adjacent along the helical molecular backbone.
- Parameter m is the effective mass of each amino acid residue. Note that variations in mass between different amino acids are ignored: the oscillatory motion is assumed to be primarily in the part of the residue common to all amino acids, as the variable part is attached laterally at the outside of the helix.

The Davydov-Scott System has a Hamiltonian form, with

$$\mathcal{H} = \sum_n -J(\psi_n^*\psi_{n+3} + \psi_{n+3}^*\psi_n) + L(\psi_n^*\psi_{n+1} + \psi_{n+1}^*\psi_n) \\ + \sum_n \frac{p_n^2}{2m} + \frac{1}{2}(q_{n+3} - q_n)^2 + (q_{n+3} - q_n)\psi_n^*\psi_n. \tag{10}$$

Aside. The main difference in the original Davydov model was assuming a symmetrical form for the interaction between the exciton and mechanical variables:

$$\sum_n (q_{n+3} - q_{n-3})\psi_n^*\psi_n.$$

Various boundary conditions can be imposed on the Hamiltonian. Defining the *bond stretchings*

$$s_n := q_{n+3} - q_n \quad (= q_{\nu+1,\alpha} - q_{\nu,\alpha}), \tag{11}$$

zero end conditions are most natural physically:
N residues indexed $0 \leq n < N$, with $\psi_n = 0$, $s_n = 0$ for "out of bounds" values of the index n.

For constructing PDE approximations via continuum limits, it is also convenient to consider an infinite chain with $n \in \mathbb{N}$ and $\psi_n \to 0,\ s_n \to 0$ as $|n| \to \infty$.

A. Approximation by a Lattice Nonlinear Schrödinger Equation

Many phenomena of interest in solutions the Davydov system are retained in the approximation that the greater stiffness of the mechanical couplings causes the exciton quantities ψ_n to interact primarily with their time average, given by the singular limit $m \to 0$.

This gives the equation herein called the *Davydov-Scott Lattice Nonlinear Schrödinger [DSLNLS] Equation*

$$\mathrm{i}\frac{d\psi_n}{dt} + J(\psi_{n+3} + \psi_{n-3}) - L(\psi_{n+1} + \psi_{n-1}) + |\psi_n|^2\psi_n = 0. \tag{12}$$

This also has Hamiltonian form, with

$$\mathcal{H} = \sum_n -J(\psi_n^*\psi_{n+3} + \psi_{n+3}^*\psi_n) + L(\psi_n^*\psi_{n+1} + \psi_{n+1}^*\psi_n) - \frac{1}{2}\sum_n (\psi_n^*\psi_n)^2. \tag{13}$$

B. Momenta (Conserved Quantities Other Than The Hamiltonian)

Charge. Both equations above have a conserved *charge* $\mathcal{E}$ (also called *exciton number* or *power* depending on the physical application). This is related to the probability density of quantum mechanics, and notably, it is quadratic:

$$\mathcal{E} = \sum_n \psi_n^*\psi_n. \tag{14}$$

This charge is associated via Noether's Theorem with a linear symmetry group action, the gauge symmetry

$$\psi_n \to \mathrm{e}^{\mathrm{i}s}\psi_n, \quad \psi_n^* \to \mathrm{e}^{-\mathrm{i}s}\psi_n^*. \tag{15}$$

Linear Momentum. The Davydov-Scott system also has a conserved momentum $\mathcal{P}$, again (degenerately) quadratic:

$$\mathcal{P} = \sum_n p_n. \tag{16}$$

This is associated via Noether's Theorem with the symmetry group action $q_n \to q_n + s$. However, conservation of linear momentum is respected by almost any reasonable time discretization (for example, any Runge-Kutta method) so little more will be said about this.

C. The NLS Continuum Limit

The nonlinearity in (8) corresponds to an effective potential $-|\psi_n|^2$, producing a "self-focusing" or "discrete self-trapping" effect that could counter dispersion and keep pulses compact and coherent over long propagation distances, akin to so-called solitons in PDE's. To seek this possible connection to solitary waves, a further approximation has been considered by Davydov, Scott et al, based on the idea that solutions might evolve into a form

that is slowly varying along spines, due to the energetic favorability given by the intra-spine coupling terms, which can be rewritten as

$$-J\sum(\psi^*_{\nu,\alpha}\psi_{\nu+1,\alpha}+\psi^*_{\nu+1,\alpha}\psi_{\nu,\alpha}),\;=J\sum|\psi_{\nu+1,\alpha}-\psi_{\nu,\alpha}|^2+2J\mathcal{E}$$

and $\frac{1}{2}(q_{\nu+1,\alpha}-q_{\nu,\alpha})^2$.

This will be seen below to require modification, but for comparison to previous work, note that the assumption of slowly varying form $\psi_{\nu,\alpha}(t)\approx\psi_\alpha(\nu\Delta x,t)$ leads to a system of three linearly coupled nonlinear Schrödinger equations

$$i\frac{\partial\psi_\alpha}{\partial t}+\frac{\partial^2\psi_\alpha}{\partial x^2}+|\psi_\alpha|^2\psi_\alpha=\hat{L}(\psi_{\alpha-1}+\psi_{\alpha+1}),$$

and then some further assumptions such as a phase shift form

$$\psi_\alpha=e^{\mathrm{i}\phi}\psi,\quad 3\phi=0\mod 2\pi$$

and suitable rescaling leads to the focusing cubic NLS equation

$$i\frac{\partial\psi}{\partial t}+\frac{\partial^2\psi}{\partial x^2}+2|\psi|^2\psi=0,$$

with robust soliton solutions

$$\psi(x,t)=A\,\mathrm{sech}(A(x-vt))\exp\left[-\frac{i}{2}(vx-(v^2/4-A^2)t)\right].$$

D. Momenta and Hamiltonian Symmetries via Invariant Quadratic Forms

Conservation of momentum and charge can be verified directly (rather than invoking Noether's Theorem) by first noting that the state variables appear in the Hamiltonian only through the *exciton products*

$$\pi_{ab}=\psi^*_a\psi_b$$

and the bond stretchings (11), all of which are invariant under the associated gauge and translation symmetries, ensuring that the Hamiltonian has these symmetries. Then direct differentiation and application of the chain rule gives

$$\frac{d\mathcal{E}}{dt}=0,\quad\frac{d\mathcal{P}}{dt}=0.$$

However it will be convenient to use a more general calculation, given in section III B.

III. TIME DISCRETIZATION METHODS THAT CONSERVE ENERGY AND MOMENTA, AND RESPECT TIME-REVERSAL SYMMETRY

The numerical methods will be described in terms of the more general Hamiltonian system

$$\frac{d\mathbf{y}}{dt} = \mathcal{J}\nabla_{\mathbf{y}}\mathcal{H}(\mathbf{y}) = \mathcal{J}\frac{\partial \mathcal{H}}{\partial \mathbf{y}}(\mathbf{y}) \tag{17}$$

with $\mathcal{J}$ an anti-symmetric matrix. One key to deriving methods that exactly conserve energy (the Hamiltonian) is to approximate (17) with a *discrete Hamiltonian system*

$$\frac{\delta \mathbf{y}}{\delta t} = \mathcal{J}\tilde{\nabla}_{\mathbf{y}}\mathcal{H}(\mathbf{y}, \mathbf{y}^+) \tag{18}$$

by defining a suitable discrete gradient approximation

$$\tilde{\nabla}_{\mathbf{y}} f(\mathbf{y}, \mathbf{y}^+) \approx \nabla_{\mathbf{y}} f(\mathbf{y}). \tag{19}$$

This can easily be done in ways that exactly conserve the Hamiltonian, but conserving other invariants (here all called *momenta*) requires an appropriate choice of the gradient approximation, and there is a natural limitation to quadratic (including linear) momenta.

Some Notation for Difference Schemes

We will focus on the time advance map for single time step, from a time t to $t+h$. Thus for a scalar variable y, a vector $\mathbf{y}$, and likewise for other variables like $\mathbf{q}$, $\mathbf{p}$, and ψ:

- $h = \delta t$ denotes the change in t over the time step.
- y alone without arguments denotes the value $y(t)$ at time t, typically the beginning of the current time step.
- $t^+ = t + h$ and y^+ denotes the value $y(t^+) = y(t+h)$.
- $\delta y = y^+ - y$.
- $\overline{y} = \dfrac{y + y^+}{2}$.

A. Energy Conserving discrete gradient methods

The basic idea, originating in the work of [15, 16] is to define a discrete approximation $\tilde{\nabla}_{\mathbf{y}} f$ of the gradient depending on values at the beginning and end of a time step

$$\tilde{\nabla}_{\mathbf{y}} f(\mathbf{y}, \mathbf{y}^+) = \left\langle \tilde{D}_1 f(\mathbf{y}, \mathbf{y}^+), \ldots \right\rangle = \left\langle \tilde{D}_{y_1} f(\mathbf{y}, \mathbf{y}^+), \ldots \right\rangle \approx \nabla_{\mathbf{y}} f(\mathbf{y}), \tag{20}$$

and then solving the above discrete Hamiltonian system. In the case of a variable matrix $\mathcal{J}(\mathbf{y})$, one instead uses an approximation $\tilde{\mathcal{J}}(\mathbf{y}, \mathbf{y}^+)$, with the natural choice being the midpoint approximation $\tilde{\mathcal{J}}(\mathbf{y}, \mathbf{y}^+) = \mathcal{J}(\overline{\mathbf{y}})$. We assume the natural consistency condition

$$\lim_{\mathbf{y}^+ \to \mathbf{y}} (\tilde{\nabla}_{\mathbf{y}} f)(\mathbf{y}, \mathbf{y}^+) = \nabla_{\mathbf{y}} f(\mathbf{y}). \tag{21}$$

A discrete gradient cannot simply be constructed from independently defined discrete approximations of the partial derivatives, because an important relation must be imposed on the components: all discrete gradients are required to satisfy the *Discrete (Multivariable) Chain Rule*

$$\delta f = (\tilde{\nabla}_{\mathbf{y}} f)(\mathbf{y}, \mathbf{y}^+) \cdot \delta \mathbf{y}. \tag{22}$$

This rule plus linearity will be imposed from now on. In fact, it will often be convenient to express discrete gradients through expressions for δf in terms of $\delta \mathbf{y}$.

Conservation of Energy With Discrete Gradient Methods

Recall the proof of conservation of energy for a Hamiltonian system: $d\mathbf{y}/dt = \mathcal{J} \nabla_{\mathbf{y}} \mathcal{H}(\mathbf{y})$

$$\begin{aligned}
\frac{d\mathcal{H}}{dt} &= \nabla_{\mathbf{y}} \mathcal{H} \cdot \frac{d\mathbf{y}}{dt} && \text{multivariable chain rule} \\
&= \nabla_{\mathbf{y}} \mathcal{H}(\mathbf{y}) \cdot \mathcal{J} \nabla_{\mathbf{y}} \mathcal{H}(\mathbf{y}) && \text{Hamilton's equations} \\
&= 0 && \text{from the anti-symmetry of } \mathcal{J}.
\end{aligned}$$

Conservation of energy is easily shown for a discrete gradient method by mimicking this argument:

$$\frac{\delta \mathcal{H}}{\delta t} = (\tilde{\nabla}_{\mathbf{y}} \mathcal{H})(\mathbf{y}, \mathbf{y}^+) \cdot \frac{\delta \mathbf{y}}{\delta t} = (\tilde{\nabla}_{\mathbf{y}} \mathcal{H})(\mathbf{y}, \mathbf{y}^+) \cdot \mathcal{J} (\tilde{\nabla}_{\mathbf{y}} \mathcal{H})(\mathbf{y}, \mathbf{y}^+) = 0.$$

B. Choosing a Discrete Gradient that Also Respects Quadratic Momenta

On the other hand, conservation of momenta, such as the charge seen above, is not automatic. Instead one must choose amongst the infinity of possible discrete gradients to satisfy conservation laws. Here the approach introduced in [17, 18] is followed, based on three facts:

1. There is a unique discrete gradient for functions of a single variable y

$$\tilde{\nabla}_y f(y, y^+) := \begin{cases} \dfrac{\delta f}{\delta y}, & y^+ \neq y \\ \dfrac{df}{dy}(y), & y^+ = y \end{cases} \tag{23}$$

   following from the chain rule requirement

$$\delta f = \tilde{\nabla}_{\mathbf{y}} f(y, y^+)\, \delta \mathbf{y}.$$

2. There is a unique time-reversal symmetric discrete gradient for a product of two variables

$$\delta(y_j y_k) = \overline{y}_j \delta y_k + \overline{y}_k \delta y_j \tag{24}$$

   which corresponds to evaluating the true gradient at the midpoint:

$$\tilde{\nabla}(y_j y_k)(\mathbf{y}, \mathbf{y}^+) = \nabla(y_j y_k)(\overline{\mathbf{y}}). \tag{25}$$

   In fact this extends to a *discrete product rule* based on

$$\delta(fg) = \overline{f}\delta g + \overline{g}\delta f. \tag{26}$$

3. Many (perhaps all) physically relevant Hamiltonian systems with conserved momenta have a natural form in which all the momenta are quadratic (including linear) functions of the state variables, and are related through Noether's theorem to a group of affine symmetries of the Hamiltonian $\mathcal{H}$, with invariance of $\mathcal{H}$ manifested by the fact that it can be expressed as a composition

$$\mathcal{H}(\mathbf{y}) = \hat{\mathcal{H}}(\mathbf{Q}) \tag{27}$$

   where each component Q_l of the new state vector $\mathbf{Q}$ is a quadratic

$$Q_l = \frac{1}{2}\sum_{j,k} A_l^{jk} y_j y_k + \sum_j b_k^j y_j, \text{ (each } A_l := \{A_l^{jk}\} \text{ symmetric)} \tag{28}$$

that is invariant under the symmetry group. For example, with the systems seen herein, the invariant quadratics with which the Hamiltonian can be expressed are the exciton products π_{ab} and the bond stretchings s_n.

The discrete Jacobian of this change of variables is given by the true Jacobian evaluated at the midpoint:

$$\tilde{D}_{\mathbf{y}}\mathbf{Q}(\mathbf{y},\mathbf{y}^+) = D_{\mathbf{y}}\mathbf{Q}(\overline{\mathbf{y}}).$$

These facts and the above chain rule requirement naturally lead to:

$$\tilde{D}_j\mathcal{H}(\mathbf{y},\mathbf{y}^+) = \sum_l \tilde{D}_l\hat{\mathcal{H}}(\mathbf{Q},\mathbf{Q}^+)\tilde{D}_jQ_l(\mathbf{y},\mathbf{y}^+) = \sum_l \tilde{D}_l\hat{\mathcal{H}}(\mathbf{Q},\mathbf{Q}^+)D_jQ_l(\overline{\mathbf{y}}), \tag{29}$$

or

$$\tilde{\nabla}_{\mathbf{y}}\mathcal{H} = \sum_l \tilde{D}_l\hat{\mathcal{H}}\ \nabla_{\mathbf{y}}Q_l, = \sum_l \tilde{D}_l\hat{\mathcal{H}}(\mathbf{Q},\mathbf{Q}^+)\ \nabla_{\mathbf{y}}Q_l(\overline{\mathbf{y}}). \tag{30}$$

Using such a discrete gradient, energy and momentum will be conserved with any choice for the factors $\tilde{D}_l\hat{\mathcal{H}}(\mathbf{Q},\mathbf{Q}^+)$. In practice, the above rules for single variable functions, products, compositions, and linearity are generally enough to construct a suitable discrete gradient for $\hat{\mathcal{H}}$.

Theorem 1 *If for a Hamiltonian system* (17)*, $\mathcal{H}$ has the form* (27) *as described above, and thus has a discrete gradient* (30)*, then numerical solution by the corresponding discrete gradient method* (18)

$$\frac{\mathbf{y}^+ - \mathbf{y}}{\delta t} = \mathcal{J}\sum_l \tilde{D}_l\hat{\mathcal{H}}(\mathbf{Q},\mathbf{Q}^+)\ \nabla_{\mathbf{y}}Q_l\left(\frac{\mathbf{y}+\mathbf{y}^+}{2}\right) \tag{31}$$

conserves the Hamiltonian and all the quadratic momenta.

The proof builds on Noether's Theorem via

Lemma 1 *Consider a Hamiltonian* (27) *given in terms of quadratics* (28) *that are invariant under a continuous symmetry group, and let Q by any of the corresponding Noetherian invariants of the Hamiltonian flow,*

$$Q = \frac{1}{2}\sum_{j,k} A^{jk}y_jy_k + \sum_j b^jy_j. \tag{32}$$

Then the following Poisson brackets vanish:

$$\{Q, Q_l\}(\mathbf{y}) := \nabla Q(\mathbf{y}) \cdot \mathcal{J}\nabla Q_l(\mathbf{y}) = 0. \tag{33}$$

Proof of Lemma 1 The quadratic Q is invariant under the flow of any Hamiltonian $\mathcal{H} = \hat{\mathcal{H}}(\mathbf{Q})$, so in particular each choice $\mathcal{H} = Q_l$. gives a Hamiltonian flow with

$$0 = \frac{dQ}{dt} = \nabla Q \cdot \mathcal{J} \nabla \mathcal{H} = \nabla Q \cdot \mathcal{J} \nabla Q_l = \{Q, Q_l\}. \tag{34}$$

Proof of Theorem 1 For any quadratic invariant of the original Hamiltonian flow, mimicking (34) gives

$$\frac{\delta Q}{\delta t} = \tilde{\nabla} Q \cdot \mathcal{J} \tilde{\nabla} \mathcal{H} = \nabla Q \cdot \mathcal{J} \sum_l (\tilde{D}_l \hat{\mathcal{H}}) \nabla Q_l = \sum_l (\tilde{D}_l \hat{\mathcal{H}}(\mathbf{Q}, \mathbf{Q}^+)) \{Q, Q_l\}(\overline{\mathbf{y}}). \tag{35}$$

Evaluating the Poisson brackets in (33) at $\overline{\mathbf{y}}$ gives $\delta Q = 0$.

C. Practical Implementation: an Iterative Solution Method

The system of equations will be nonlinear (unless the Hamiltonian system itself is linear), so we need an iterative solution method. The following method exploits the quasi-linearity of the system to preserves linear stability properties and exact momentum conservation without the cost of a full quasi-Newton method: Construct successive approximations $\mathbf{y}^{(k)}$ of $\mathbf{y}^+$ by solving

$$\frac{\mathbf{y}^{(k)} - \mathbf{y}}{\delta t} = \mathcal{J} \sum_l \tilde{D}_l \hat{\mathcal{H}}(\mathbf{Q}, \mathbf{Q}^{(k-1)}) \, \nabla_{\mathbf{y}} Q_l \left(\frac{\mathbf{y} + \mathbf{y}^{(k)}}{2} \right), \tag{36}$$

where $\mathbf{Q}^{(k)} := \mathbf{Q}(\mathbf{y}^{(k)})$. Initialization can be with $\mathbf{y}^{(0)} = \mathbf{y}$ or some other suitable approximation of $\mathbf{y}^+$. That is, the nonlinear part $\tilde{\nabla}_{\mathbf{Q}} \hat{\mathcal{H}}$ is approximated using the current best available approximation $\mathbf{y}^{(k-1)}$ of $\mathbf{y}^+$, while the linear terms are left in terms of the unknown $\mathbf{y}^{(k)}$ to be solved for. This equation is linear in the unknown $\mathbf{y}^{(k)}$, making its solution straightforward, and much as above, we have:

Theorem 2 *Each iterate $\mathbf{y}^{(k)}$ given by the above scheme* (36) *conserves all quadratic first integrals that are conserved by the original discrete gradient scheme* (31).

The proof is as for Theorem 1 above except that the Poisson brackets are evaluated at $\left(\mathbf{y} + \mathbf{y}^{(k)}\right)/2$.

Energy is of course only conserved in the limit $k \to \infty$. However, iterating until energy is accurate within machine rounding error is typically practical: if this take too many iterations, it is better for overall accuracy to reduce the time step size δt to speed the convergence.

Unconditional Linear Stability Another advantage of this approach to iterative solution is that it has unconditional linear stability, since for a linear system, $\tilde{D}_{\mathbf{Q}}\hat{\mathcal{H}}$ is constant, the scheme converges in a single iteration, and is the A-stable implicit midpoint method.

D. Higher Order Accuracy by Symmetric Step Composition

The methods seen so far are only second order accurate in time. Fortunately, the method of *symmetric step composition*, developed in [19–22] for use with symplectic methods, and reviewed in the book [23], gives a systematic way to construct methods of any higher even order while preserving all the interesting properties: conservation of the Hamiltonian and quadratic invariants, and time-reversal symmetry.

Numerical results are computed below using the fourth-order accurate Suzuki method [23, Example II.4.3, p. 45], composing five steps of lengths $\gamma_j \delta$,

$$\gamma_1 = \gamma_2 = \gamma_4 = \gamma_5 = \frac{1}{4 - \sqrt[3]{4}}, \quad \gamma_3 = 1 - 4\gamma_1.$$

E. Aside: Comparison to Symplectic Methods

The most commonly used conservative methods for Hamiltonian systems are symplectic methods such as the implicit midpoint method which conserve momenta, but cannot in general conserve energy, as described by a theorem of [24]. For the systems here that are not in classical mechanical form $\mathcal{H}(\mathbf{q}, \mathbf{p}) = K(\mathbf{p}) + U(\mathbf{q})$, the main choices are the midpoint method itself, high order diagonally implicit Runge-Kutta methods (which are all given by symmetric composition of midpoint steps), and fully implicit Gaussian methods.

All but the last are cognates of the energy-momentum methods described here, reducing to the same form for linear equations, with the main difference being exact conservation of energy. Gaussian symplectic methods are desirable when the time step size is small enough to allow their solution by simple fixed point iteration, but are not cost effective for stiff systems where an unconditionally stable iterative method such as that above must be used.

IV. NUMERICAL RESULTS

It seems most likely that the initial excitation will occur at a single residue so that the initial data is very far from the slowly varying form expected of a continuum limit. Thus the question addressed here, as in earlier work like [3, 5], is whether such initial data is likely to lead to a form that can be well approximated by a smooth function of position, leading to a hopefully more tractable PDE model. It will be seen that some significant parts of the solution do fit a continuum limit, but instead of the integrable NLS model seen in the work of Davydov and Scott, they relate to a third derivative NLS equation and the Airy PDE, as discussed in Section V.

A. Davydov-Scott System With Impulsive Initial Data

The main case studied is initial data with excitation at a single residue n_0:

$$\psi_{n^*}(0) = A, \quad \psi_n(0) = 0 \text{ for } n \neq n_0, \tag{37}$$

which seems physical plausible, given that the likely source of excitation is the transfer of energy from the ATP-ADP reaction to a vibrational excited state in one C=O bond. Zero initial data is used for the mechanical terms:

$$q_n(0) = p_n(0) = 0.$$

In addition to solving with the physically correct parameter values given above, the limit $m \to 0$ is explored by comparing to solutions with far smaller value $m = 10^{-6}$, and with the $m = 0$ approximation DSLNLS in (8).

B. Time step choice and handling of the faster mechanical terms

The choice of time steps here is always constrained by

$$\delta t \leq \min\left(\frac{1}{2(J+L)}, \frac{1}{\omega}\right)$$

which satisfies the natural accuracy and stability requirements for explicit methods and for convergence of a simple fixed point iterative method. While this is confirmed to give accurate solutions in the sense that all graphs here are completely indistinguishable from

results with any smaller time step size, far more is in fact true: with all graphs presented relating only the exciton variables, the graphical results are visually identical for any time step sizes

$$\delta t \leq \frac{1}{2(J+L)}$$

depending only on the time scale manifested in the exciton evolution equation. Thus the time discretization is effectively handling any faster time scales in the mechanical variables in the innocuous way that one hopes for stiff modes to be handled by an unconditionally stable method, with no adverse effect on the accuracy of the more slowly evolving variables.

C. Observations with an initial impulse at one residue

Figures 1 and 2 show the results for initial data as in (37) with $A = 2$ at the end of the molecule: $n^* = 0$. (The "molecule" has an unnaturally large 3000 residues, to allow longer term trends to be seen more clearly.)

A large portion of the initial excitation travels at roughly constant speed in a fairly coherent pulse, with far less dispersion than one would expect for a linear wave equation. In the forward half of the pulse, the amplitude is slowly varying, suggesting the possibility of a continuum limit description for part, but not all, of the solution. In these respects, the result is similar to those of [3], which however used a 200 residue molecule, a shorter time, and the two-point initial impulse form $\psi_0(0) = \psi_1(0) = A$, $\psi_n(0) = 0$ for $n > 1$. Another noteworthy fact is that the region with slow change of amplitude between residues ends at almost exactly half way between the leading edge of the pulse and its origination point. This is as yet unexplained.

However, slow variation is not seen in ψ_n, due to rapid phase variation: this is true even if one restricts to individual spines. This is seen by examining the real or imaginary parts along any spine or along all residues, as for example in Figure 3 for the spine $\alpha = 0$.

On closer examination, there is an approximate periodicity of period four in phase, which is revealed by examining the phase-shifted quantity $w_n = \mathrm{i}^n \psi_n$, as in Figure 4. It is now truly slowly varying over the front half of the pulse, from residue 270 forward. This pattern is seen over a wide variety of impulsive initial data, varying amplitude A, using an impulse on the first one or two residues, and also with an initial impulse at another residue along the molecule. For example, Figure 5 shows a right-going pulse in w_n at $t = 40$, generated

by an initial impulse of amplitude $A = 2$ at residue $n^* = 900$. (There is a near identical left-going pulse, of course.)

D. Smaller m and the limit $m \to 0$

The small mass and zero mass approximations work well. For example, with the same initial conditions as in Figures 1–4 with the only change being setting $m = 10^{-6}$ instead of its physical value 0.0069 (and reducing the time step size to $\delta t = 0.0005$), the quantity w_n is seen in Figure 6. The values are almost identical to the corresponding ones for the $m \to 0$ limit equation DSLNLS (8), as shown in Figure 7. In all cases:

- Wherever there is slow variation in the amplitudes ψ_n, there is slow variation in residue index n of the w_n, and not of the ψ_n, even if one considers only values $\psi_{m,\alpha}$ within a single spine α.
- The behavior of w_n for the original Davydov-Scott system is well approximated by that in the LNLS approximation (8).
- The leading pulse with slow variation moves at a speed of approximately 12.8 residues per unit time.

V. THE THIRD DERIVATIVE NLS CONTINUUM LIMIT

These observations can be partially explained by analysis of the dispersion relation for the linearization, and lead to consideration of a continuum limit for the transformation of (8) into an equation for the w_n. This is closely related to work of [25] and [26] on similar lattice NLS equations, with the main difference being that they address LNLS systems with only nearest-neighbor exciton dipole interactions: effectively $J = 0$.

A. Dispersion Analysis and Phase Shift Along the Chain

Consider the linear part of equation (8)

$$\mathrm{i}\frac{d\psi_n}{dt} + J(\psi_{n+3} + \psi_{n-3}) - L(\psi_{n+1} + \psi_{n-1}) = 0. \tag{38}$$

and seek discretized traveling waves of the form

$$\psi_n = \phi(z)\mathrm{e}^{\mathrm{i}(\beta n+\omega t)}, \quad z = n - vt, \quad \phi(z) = \mathrm{e}^{\mathrm{i}kz}$$

with an emphasis on slow variation along the chain, indicated by small values of k. This gives the dispersion relation

$$\omega(k) = kv + 2J\cos(3(k+\beta)) - 2L\cos(k+\beta). \tag{39}$$

As shown by Pelinovsky and Rothos [25], using center manifold and normal form techniques (following earlier work of Iooss and Kirchgassner [27, 28] for the FPU and Klein-Gordon lattices) and using the "tail analysis" of Flach and Kladko [29], nonlinear solutions can bifurcate from solutions of this linear part at inflection points of (39), in particular $\omega'(0) = 0$ at $k = 0$ for the slowly varying solutions of interest here. This gives group velocity

$$v = 6J\sin(3\beta) - 2L\sin(\beta).$$

Maximum signal speeds in each direction

$$v_{max} = \pm(6J + 2L)\ [\,= \pm 13 \text{ for the parameter values above}]$$

occur at the triple roots $\beta = \mp\pi/2$ of the dispersion relation.

Aside: This is the main point where the detail of the lattice structure are important: specifically, that the "stride" in the coupling terms is odd. Behavior is different for a helix with an even number of residues per twist, though a near constant phase shift $\mathrm{e}^{\mathrm{i}\beta}$ along the chain is still seen in numerical simulations, for somewhat different values of β.

The right-going case $v = 6J + 2L$, $\beta = -\pi/2$ corresponds to small amplitude solutions of the form $\psi_n \approx (-\mathrm{i})^n\phi(z)\mathrm{e}^{\mathrm{i}\omega t}$. for which

$$w_n(t) = (\mathrm{i})^n\psi_n(t) \approx \mathrm{e}^{\mathrm{i}(k(n-vt)+\omega t)} \tag{40}$$

is slowly varying along the lattice.

B. Approximation by the Third Derivative Nonlinear Schrödinger Equation

Both the numerical observations and the above analysis suggest considering a continuum limit for the phase-shifted quantities $w_n(t)$. Rewriting (8) in terms of these gives

$$\frac{dw_n}{dt} + J(w_{n+3} - w_{n-3}) + L(w_{n+1} - w_{n-1}) = \mathrm{i}|w_n|^2 w_n \tag{41}$$

as the starting point for such a continuum limit. Next, expanding in the limit of a slowly varying solution

$$w_n(t) \approx \sqrt{\epsilon} w(z, \tau), \quad z = k(n - vt), \tau = \epsilon t \tag{42}$$

where $v = 6J + 2L$ as above, $\epsilon = (1/3)\kappa k^3$, and $\kappa = (27J + L)$, gives

$$w_\tau + w_{zzz} = \mathrm{i}|w|^2 w + O(k^2).$$

Slow variation between consecutive nodes is indicated by $k \ll 1$, which leads to approximation by the *third derivative nonlinear Schrödinger equation*

$$\frac{\partial w}{\partial \tau} + \frac{\partial^3 w}{\partial z^3} = \mathrm{i}|w|^2 w. \tag{43}$$

The continuum limit for the linearization considered above is

$$\frac{\partial w}{\partial \tau} + \frac{\partial^3 w}{\partial z^3} = 0, \tag{44}$$

known as the Airy PDE (but also called the "Airy Diffusion Equation", though it not diffusive). This has a slowly decaying and spreading fundamental solution with initial impulse at $z = z_0$, in terms of the Airy function Ai (see graph Airy_Functions.svg at Wikimedia Commons):

$$w(z, \tau) = \frac{1}{(3\tau)^{(1/3)}} \mathrm{Ai}\left(\frac{z - z_0}{(3\tau)^{(1/3)}} \right). \tag{45}$$

Converting back via (42) with $z_0 = kn_0$ to place the initial impulse at residue n_0 gives approximate solution

$$w_n(t) \approx \frac{\sqrt{k}\,\kappa^{1/6}}{\sqrt{3}\,t^{1/3}} \mathrm{Ai}\left(\frac{(n - n_0) - vt}{(\kappa t)^{1/3}} \right). \tag{46}$$

C. Nonlinear Effects: Deviation from Airy Function Pulse Form and Evidence of Self-focusing

The approximate solutions arising the above linearized continuum model have some notable features:

- Approximately traveling wave form, of speed $v = 6J + 2L = 13$.
- Airy function profile.
- Slow decrease in amplitude and broadening, with time scale $t^{1/3}$.

This speed is a good match for the values observed for the Davydov-Scott system, and the Airy function form is a good approximation for small initial amplitude, as is the slow temporal decrease in amplitude.

The most noteworthy deviations as initial amplitude is increased are that the leading "hump" becomes more dominant (and so more similar to a sech pulse), and that its does not continue to spread in width and decrease in height at rate $t^{1/3}$. Instead, it appears to stabilize in width. Perhaps this is the familiar control of dispersion by nonlinear self-focusing or "self-trapping", but any such analysis remains to be done.

VI. CONCLUSIONS

1. The sustained traveling exciton pulses seen in Davydov-style exciton-oscillator model of energy propagation in α-helix protein are well modeled by the "slow exciton" approximation by a lattice NLS equation.

2. As noted by other authors, the main part of the pulse has magnitude $|\psi_n|$ that varies slowly, allowing a PDE continuum limit approximation.

3. However, the phase of the ψ_n varies rapidly in index n, by a quarter turn at each step, and thus the slow spatial variation is instead in $w_n = (\mathrm{i})^n \psi_n$, leading to a new continuum limit approximation by the third derivative nonlinear Schrödinger equation $w_\tau + w_{zzz} = \mathrm{i}|w|^2 w$.

4. Solutions for this bifurcate off from those of its linearization, the Airy PDE $w_\tau + w_{zzz} = 0$, and retain a resemblance to the slowly modulated traveling wave solutions of that equation in terms of the Airy function even when the nonlinear term is of significant magnitude.

5. Evidence of nonlinear "self-focusing" or "self-trapping" effects are seen, in that the leading hump of the pulse remains stronger and narrower as time increases than those of the linearization, supporting the more sustained propagation, despite the loss of the exact NLS sech soliton structure proposed in previous studies.

6. The higher order exactly energy-momentum conserving time-discretization method used is seen to handle well the stiffness that can arise in such systems, making it a

good candidate for similar problems, including spatial discretization of various stiff nonlinear dispersive PDE's.

[1] A. S. Davydov, *Theory of Molecular Excitations* (Plenum press, New York, 1971).

[2] A. S. Davydov and N. I. Kislukha, Phys. Status Solidi B **59**, 465 (1973).

[3] A. C. Scott, Physica Scripta **25**, 651 (1982).

[4] A. C. Scott, Phys. Rev. A **26**, 578 (1982).

[5] A. C. Scott, Physica Scripta **29**, 279 (1984).

[6] A. S. Davydov, *Biology and Quantum Mechanics* (Pergamon Press, New York, 1982).

[7] A. C. Scott, Physics Reports **217**, 1 (1992).

[8] Z. Ivić, Physica D **113**, 218 (1998).

[9] J. Tekić, Z. Ivić, S. Zeković, and Z. Przulj, Phys. Rev. E **60**, 821 (1999).

[10] D. Čevisović, A. Reshetnyak, S. Galović, and Z. Ivić., "On the vibron dressing in the one–dimensional macromolecular chains caused by the interaction with acoustic phonon modes," (2012), appeared online 10 April 2012, arXiv:1204.2243v1.

[11] A. S. Davydov, Physica D **3**, 1 (1981).

[12] A. S. Davydov, *Solitons in Molecular Systems* (Kluwer Academic Publishers, Dordrecht, 1991).

[13] T. Holstein, Ann. Phys. **8**, 326 (1959).

[14] T. Holstein, Ann. Phys. **8**, 343 (1959).

[15] O. Gonzales, Journal of Nonlinear Science **6**, 449 (1996).

[16] O. Gonzales and J. C. Simo, Comput. Methods Appl. Mech. Eng. **134**, 197 (1996).

[17] B. LeMesurier, Mathematics and Computers in Simulation **82**, 1239 (2012), published online 30 December 2010.

[18] B. LeMesurier, Physica D **241**, 1 (2012), published online 1 Oct 2011.

[19] M. Creutz and A. Gocksch, Phys. Rev. Lett. **63**, 9 (1989).

[20] E. Forest, AIP Conference Proceedings **184**, 1106 (1989).

[21] M. Suzuki, Phys. Lett. A **135**, 319 (1990).

[22] H. Yoshida, Phys. Lett. A **150**, 262 (1990).

[23] E. Hairer, C. Lubich, and G. Wanner, *Geometric Numerical Integration: Structure Preserving Algorithms for Ordinary Differential Equations*, 2nd ed. (Springer, 2006).

[24] Z. Ge and J. E. Marsden, Phys. Lett. A **133**, 134 (1988).

[25] D. Pelinovsky and V. Rothos, Physica D **202**, 16 (2005).

[26] P. G. Kevrekidis, S. V. Dmitriev, and A. A. Sukhorukov, Mathematics and Computers in Simulation **74**, 343 (2007).

[27] G. Iooss, Nonlinearity **13**, 849 (2000).

[28] G. Iooss and K. Kirchgassner, Comm. Math. Phys. **211**, 439 (2000).

[29] S. Flach and K. Kladko, Physica D **127**, 61 (1999).

FIGURES

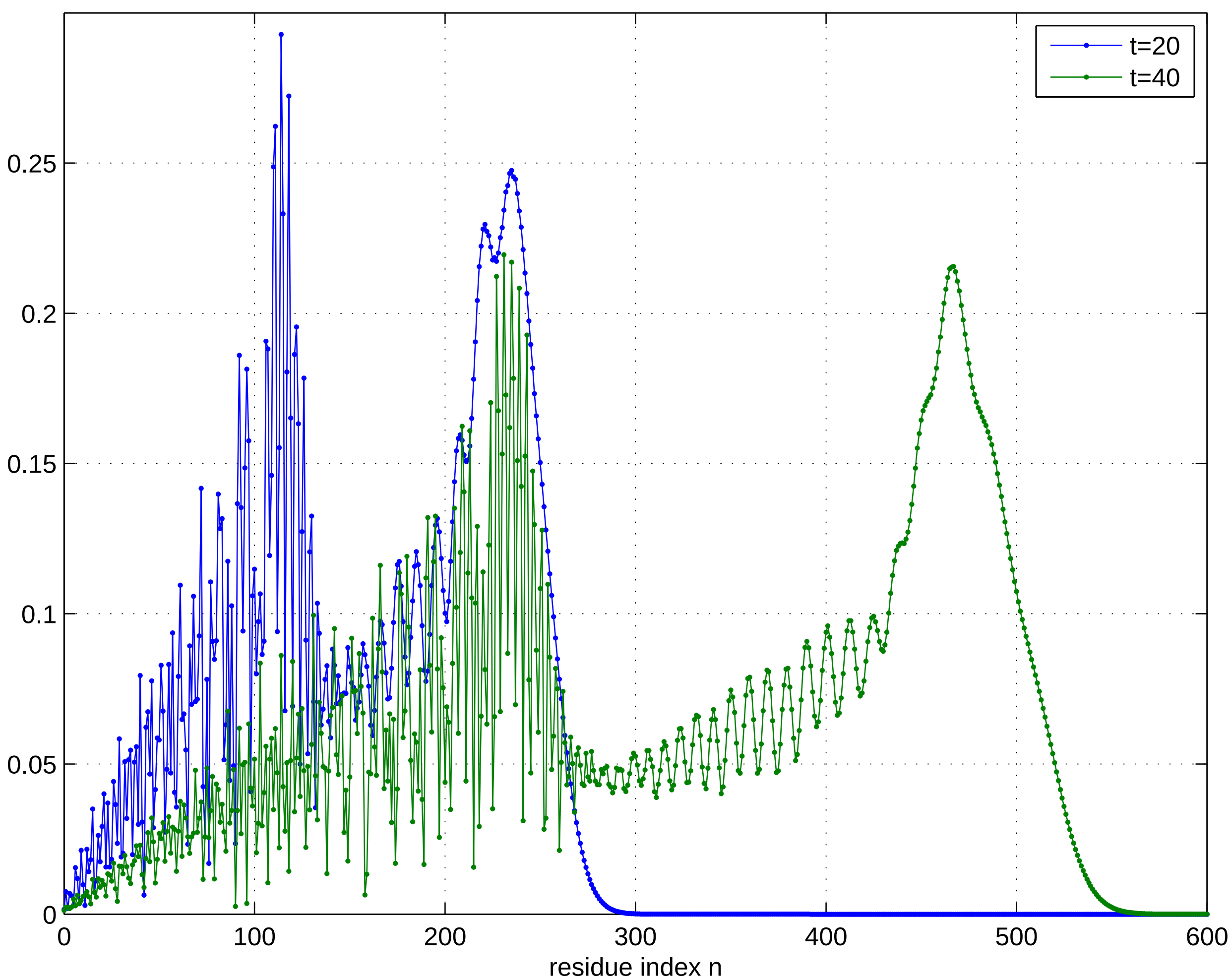

FIG. 1. Davydov-Scott system, $A = 2$ impulse initial data at residue 0: $|\psi_n|$ at times $t = 20, 40$. ($\delta t = 0.01$.)

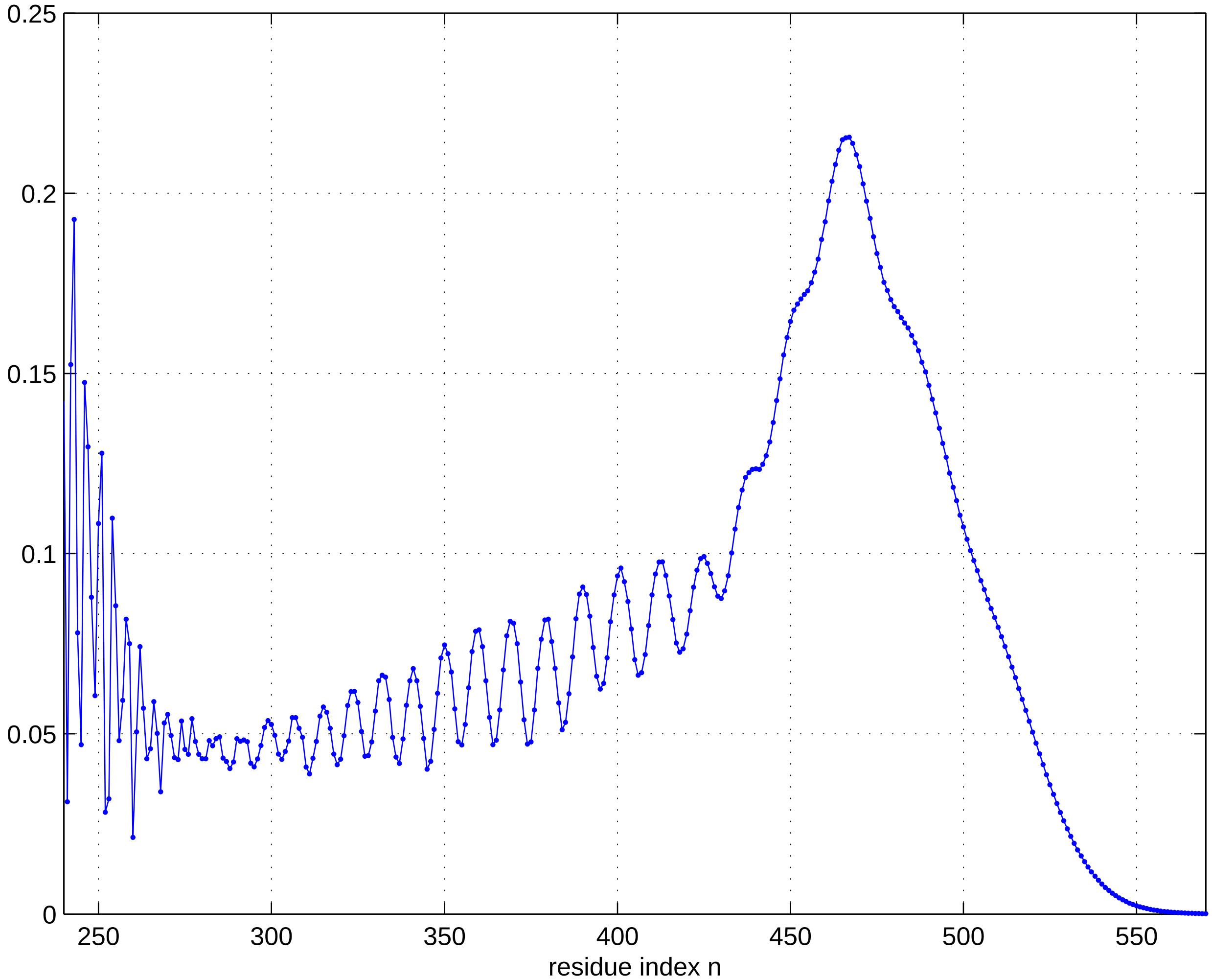

FIG. 2. As above, $t = 40$ only: enlarged view of leading pulse amplitude.

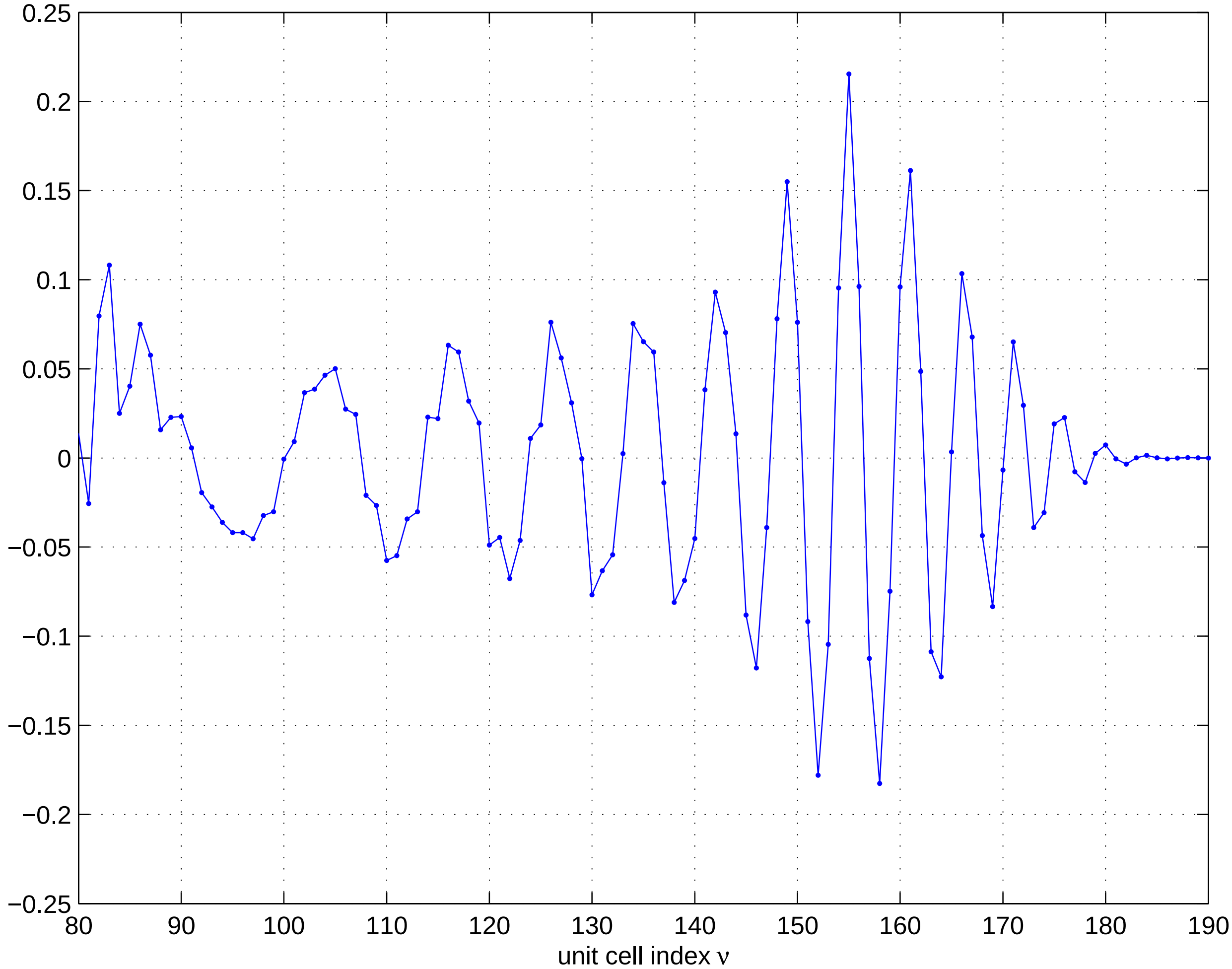

FIG. 3. $\Re(\psi_{\nu,0})$: real parts on spine $\alpha = 0$; initial data as above.

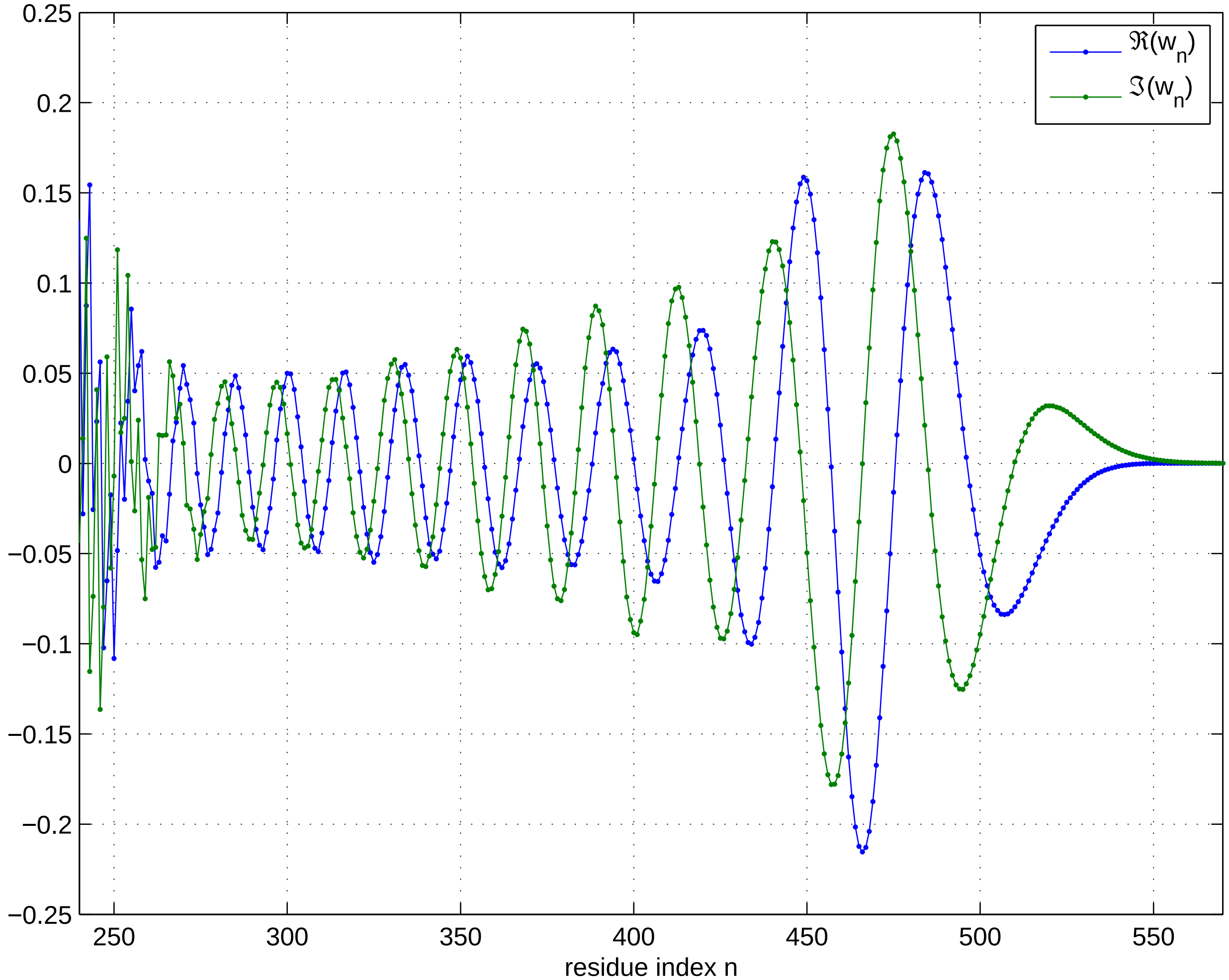

FIG. 4. Real and imaginary parts of $w_n = \mathrm{i}^n \psi_n$; initial data as above.

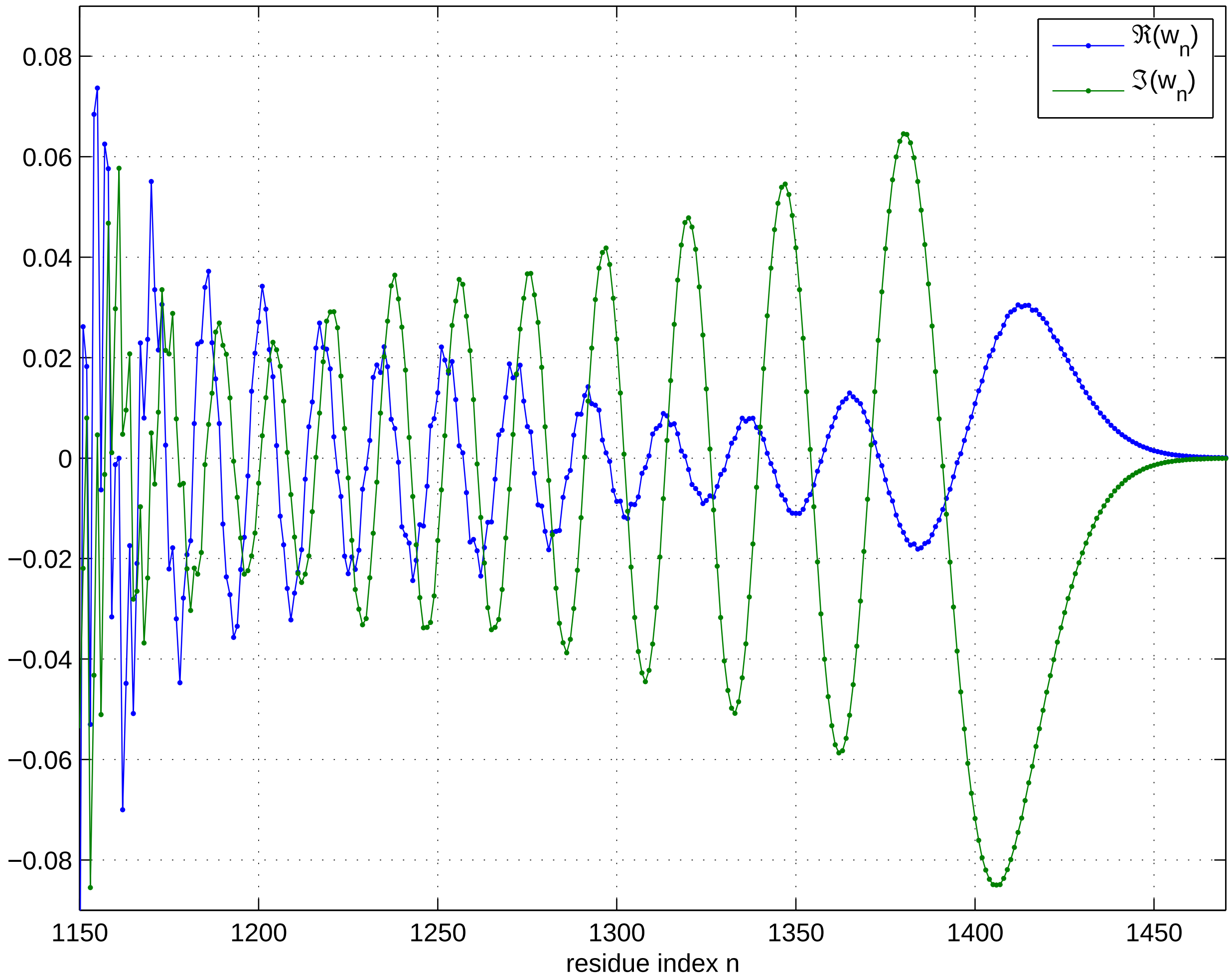

FIG. 5. Real and imaginary parts of $w_n = \mathrm{i}^n \psi_n$ at $t = 40$ for initial impulse $A = 2$, $n^* = 900$.

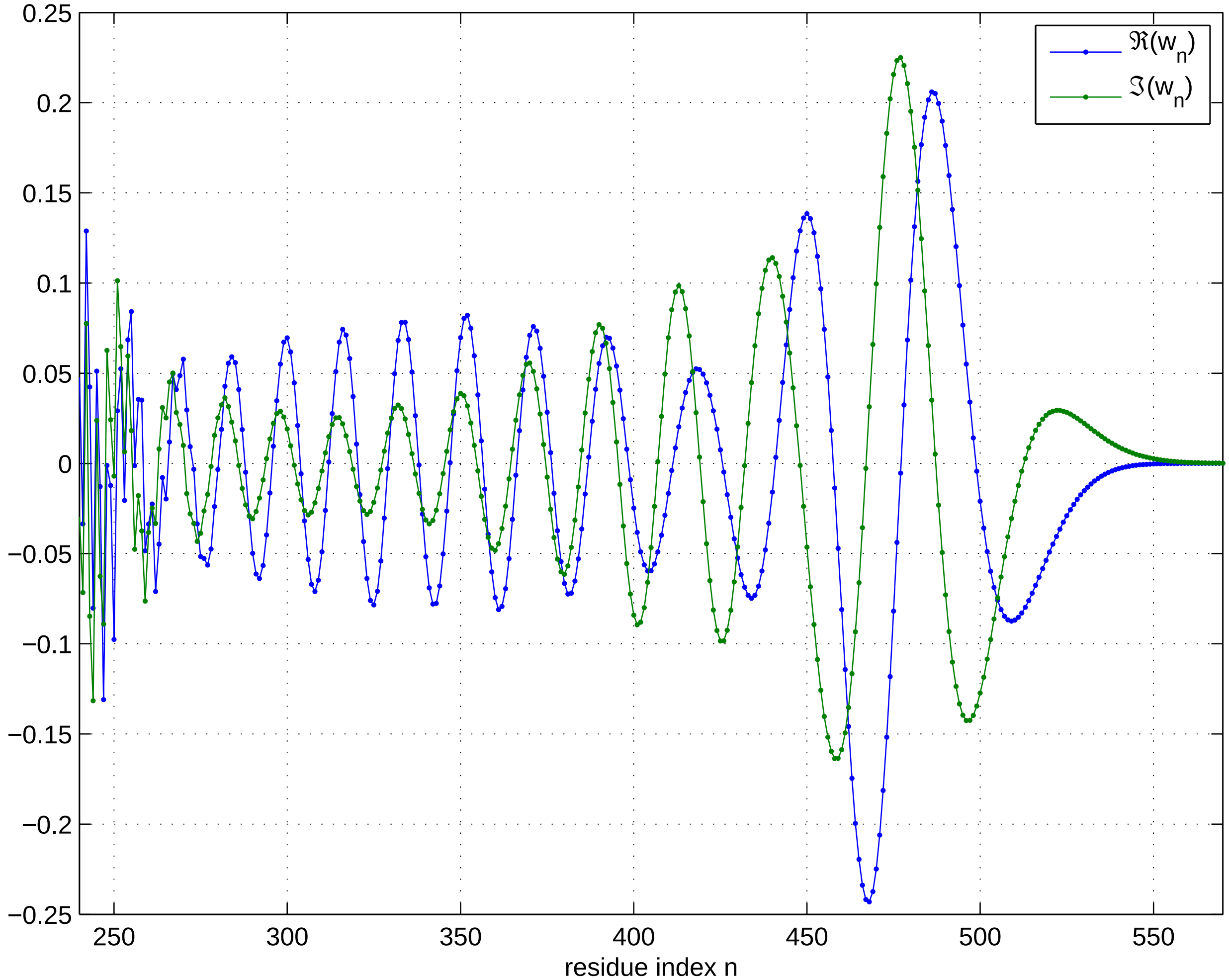

FIG. 6. As in Figure 4 except with far smaller mass $m = 10^{-6}$, $\delta t = 0.0005$.

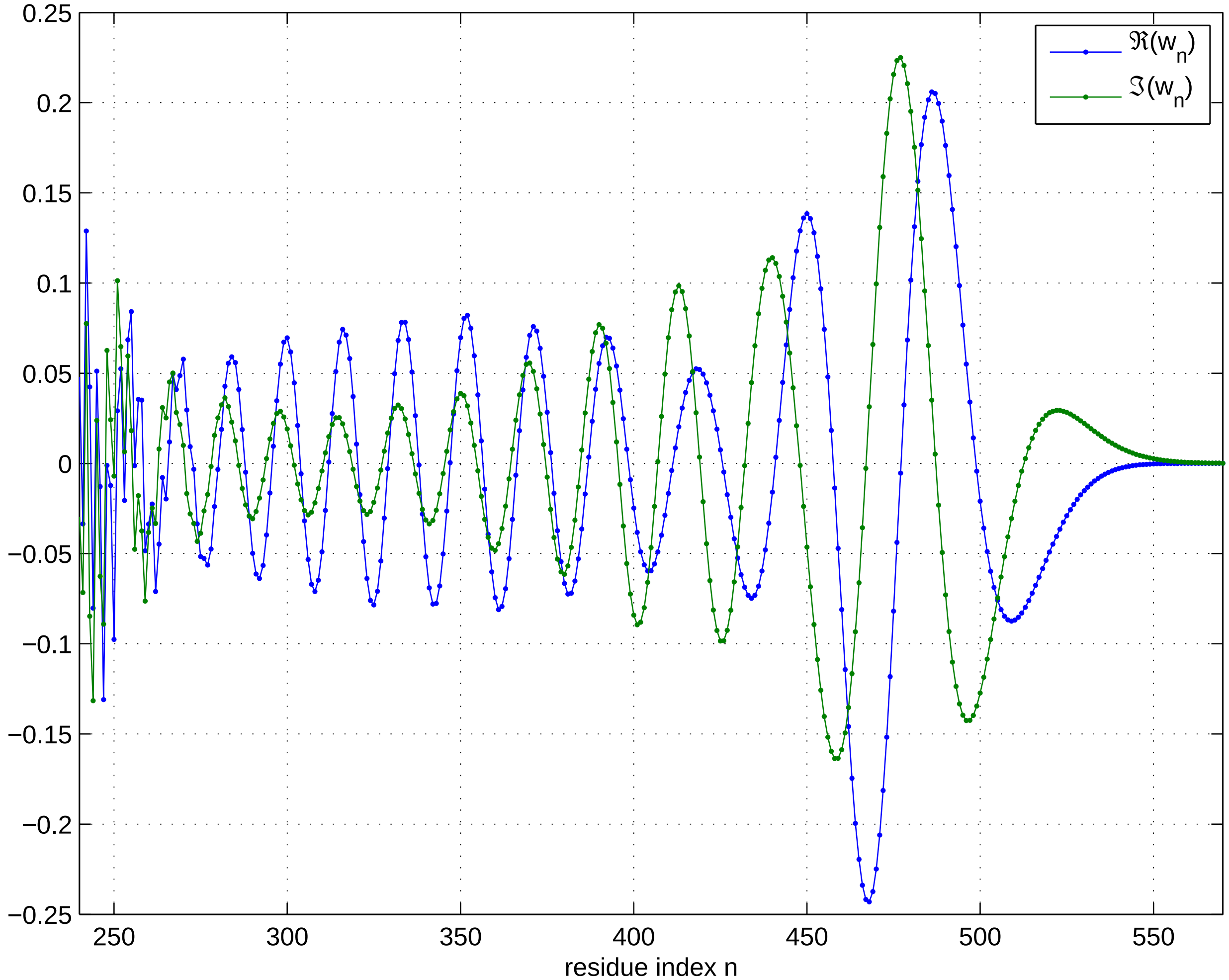

FIG. 7. As in Figures 4 and 6 but for the DSLNLS equation.